ETH-Bibliothek Zürich, E-Periodica, https://www.e-periodica.ch

Cathodoluminescence spectroscopy and the orientation of a hydrothermal quartz crystal

by *Pierre A. Picouet* [1]

Abstract

This paper examines the possible changes in the cathodoluminescence emission of a hydrothermal quartz crystal prepared following two directions, parallel and perpendicular to the crystallographic c-axis. Experiments were conducted on an optical cathodoluminescence detection system coupled to a scanning electron microscope at room temperature. Results included spectra analysed with a summation of Gaussian curves, cathodoluminescence signal evolution with electron beam exposure time and spectral comparison with the analytical surface. Results demonstrated that the difference between the two orientations depend upon the experimental conditions, such as acceleration voltage, sample current, analytical surface and room temperature.

Keywords: cathodoluminescence, quartz, c-axis, orientation.

Introduction

In the last decade several articles have described the cathodoluminescence (CL) signal of quartz and tried to interpret it (ZINKERNAGEL, 1978; MATTER and RAMSEYER, 1985; RAMSEYER et al., 1988; OWEN, 1991; STEVENS-KALCEFF and PHILLIPS, 1995; BRUHN et al., 1996; DEMARS et al, 1996; GORTON et al., 1997, HABERMANN et al., 1999).

In a previous work at the University of Fribourg, in collaboration with the University of Bordeaux III, a methodology was developed to compare quartz grains included in archaeological ceramics (PICOUET, 1997; PICOUET et al., 1999). Quartz grains in clay ceramic have a random orientation in respect to their c-axis. Therefore the orientation (perpendicular or parallel to c-axis) of a quartz crystal may be an important consideration for the interpretations and the use of CL emission for archaeometric purpose. A recent publication by GORTON et al. (1997) shows that CL emission of ultra pure hydrothermal quartz can change at low temperature (100–200 °K) if measurements are carried out perpendicular or parallel to the c-axis. The aim of this paper is to verify if the orientation of the quartz crystal affects the CL signal under experimental conditions such as an acceleration voltage of 20 kV, a sample current of 0.15 μA, an analytical surface (S) of 0.013 mm^2 and at a room temperature of 298 K (PICOUET, 1997; PICOUET et al., 1999).

A natural hydrothermal quartz crystal (PP40) from the Gotthard massif (near Kastelhorn, Ticino, Switzerland) in the Swiss Alps was taken. The single crystal was cut parallel to the c-axis (PP40-C) and perpendicular to the c-axis (PP40-H).

Research equipment

Analyses on the quartz crystal were made with a JEOL 820 scanning electron microscope (SEM) coupled with an optical detection system with an ellipsoid mirror collecting the signal inside the analysis chamber and sending it to a HRS2 Jobin-Yvon monochromator with 1200 grooves/mm by mirrors and a polarised fibre optic. A Hamamatsu R943-02 photomultiplier was used to record the CL signal.

The results are plotted as spectra in the energy range of 1.55 eV (800 nm) to 3.54 eV (350 nm). The measurements were started at 350 nm with a speed of 5/3 $nm.s^{-1}$ summing to an acquisition time of 300 seconds. For an acquisition of the evolution

[1] Institut de Minéralogie et Pétrographie, Université de Fribourg, Pérolles, CH-1700, Fribourg, Switzerland. Present address: Optoelectronics Research Center, School of Applied Sciences, The Robert Gordon University, Blackfriar Street Building, Schoolhill, Aberdeen, AB10 1FR, U.K. <p.picouet@rgu.ac.uk>

in time, a single wavelength is selected using the monochromator. The experimental conditions were as follows: Acceleration voltage 20 kV, sample current 0.15 μA and working distance of 14 to 16 mm. The analytical surface (S) was from 0.3 mm^2 to 0.0018 mm^2 and experiments were conducted at room temperature (298 °K). All spectra were corrected for the efficiency of the detection system and samples were polished thin sections coated with carbon.

Results

Three different types of analysis were conducted. Firstly the CL spectrum of each sample under the same analytical conditions were obtained in wavelength scale, converted to energy scale (eV unit) and fitted with a sum of gaussian functions. Secondly the evolution of CL signal of both samples with beam exposure time were compared and at least two spectra were recorded. Thirdly the CL signal of both samples was compared in relation to the size of the analytical surfaces (S) which is correlated with the current density.

Figure 1 shows the CL spectra normalised at 1000 arbitrary units of the two samples at a magnification of x1000 (S = 0.013 mm^2). Both spectra are similar (Fig. 1b) and exhibited a principal component, of orange-red luminescence centered at 625–685 nm (1.98–1.81 eV) and a less intense
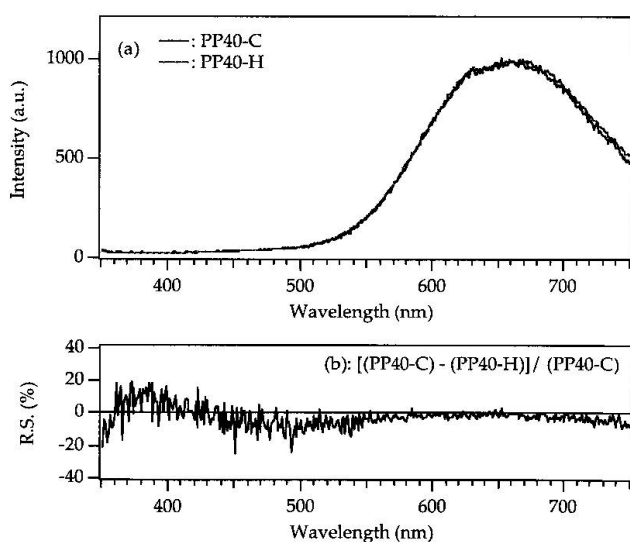

Fig. 1 (a) Cathodoluminescence spectra of a natural quartz PP40-C and PP40-H. The grey areas show the red component (625–685 nm) and the blue one (430–500 nm). (b) The curve represents the relative subtraction (R.S.) between the intensity PP40-C minus the intensity of PP40-H divided by the intensity of PP40-C. The magnification is x1000 and the analytical surface S is 0.013 mm^2.

blue luminescence component centered at 430–500 nm (2.88–2.48 eV). As shown in table 1 and figures 2a and 2b, each component is a combination of at least two emission bands; for the red component there is the principal emission band near 1.88 eV (661 nm) and another band at 2.00 eV (620 nm). For the blue component, according to previous experience (PICOUET, 1997) and literature (STEVENS-KALCEFF and PHILLIPS, 1995), three emission bands can be used in the fitting process: near 3.20 eV (388 nm), 2.76 eV (448 nm) and 2.43 eV (511 nm). An additional emission band between 2.09 eV (592 nm) and 2.15 eV (576 nm) is also used. These results are consistent with the literature (LUFF and TOWNSEND, 1990, MUNEKUNI et al., 1990; RAMSEYER and MULLIS, 1990; REMOND et al., 1992; STEVENS-KALCEFF and PHILLIPS, 1995; GORTON et al., 1997).

According to publications (LUFF and TOWNSEND, 1990; MUNEKUNI et al., 1990; RAMSEYER and MULLIS, 1990; REMOND et al., 1992; STEVENS-KALCEFF and PHILLIPS, 1995), red emission bands at 1.88 and 2.00 eV are associated with NBOHC (Non Bonding Oxygen Hole Center on [SiO$_4$]$^+$) defects (IKEYA, 1993). The blue emission band near 2.76 eV is associated with a radiation recombination of a E$_1$' center ([SiO$_3$]$^+$). The defect structure associated with the green-blue band near 2.43 eV has not been determined but it is related with extrinsic defects. The yellow-green band at 2.09–2.15 eV can be related to a germanium (Ge) impurity associated center ([GeO$_4$/Li]$^\circ_c$). The ultraviolet band near 3.20 eV can be related with an aluminium (Al) impurity associated center ([AlO$_4$]$^\circ$). We do recognise that element analysis is required to complete the interpretation for these bands and currently we are working on it.

In accordance with published papers (ZINKER-NAGEL, 1978; RAMSEYER et al.,1988; RAMSEYER and MULLIS, 1990; REMOND et al., 1992; STEVENS-KALCEFF and PHILLIPS, 1995; STEVENS-KALCEFF et al., 1996; HABERMANN et al., 1999), our experiments showed that the luminescence of quartz changes with beam exposure time (Figs 3 and 4). The evolution does not follow the same trends as the intensity of the blue component (2.76 eV => 450 nm) decreases rapidly during the first 10–20 seconds and reach after a stationary area while the red component (1.88 eV => 650 nm) intensity increases rapidly during the first 5–20 seconds and becomes linear afterwards.

Figure 3 shows that although the evolution of the red component is similar for both samples there is some difference during the first 30 seconds: the curve of the sample PP40-C increases very rapidly (five times) during the first 4 seconds with time and then rests at a saturation "plateau"

Tab. 1   Mean CL emission positions of the two samples PP40-C and PP40-H and origin of the band emission according to the literature. For each sample four spectra have been fitted.

PP40-C		PP40-H		Intensities (a.u.)	Suggested interpretation
position (eV)	width (eV)	position (eV)	width (eV)		
1.88 ± 0.01	0.39 ± 0.01	1.87 ± 0.01	0.40 ± 0.01	(985)	non-bridging oxygen hole center (NBOHC)[1],[4] or associated with oxygen vacancies[2],[3].
2.01 ± 0.01	0.07 ± 0.001	2.00 ± 0.01	0.07 ± 0.01	(43)	nonbridging hydroxy precursor third type of NBOHC precursor ?[1]
2.09 ± 0.04	0.29 ± 0.07	2.15 ± 0.01	0.23 ± 0.06	(71)	radiative recombination of a self trap exciton[4], or Germanium impurity [1],[2]
2.41 ± 0.04	0.37 ± 0.06	2.45 ± 0.04	0.29 ± 0.04	(42)	extrinsic emission [2],[4],
2.77 ± 0.05	0.39 ± 0.05	2.76 ± 0.05	0.29 ± 0.04	(27)	radiative recombination of an exciton associated with E_1' center [4],
3.26 ± 0.08	0.48 ± 0.09	3.13 ± 0.08	0.40 ± 0.07	(22)	impurity associated center of $[Al^{3+}\text{-}M^+]$. M^+ can be Li^+, H^+ [2],[4],[3].

(1): MUNEKUNI *et al.*, 1990; (2): LUFF & TOWNSEND, 1990; (3): REMOND *et al.*, 1992; (4): STEVENS-KALCEFF & PHILLIPS, 1995.

after which there is a linear increase. In the case of sample PP40-H the red signal was much slower in reaching the linear stage. A calculation of the linear evolution in both samples gives:

$I(t) = (1.73 \pm 0.02).t$ for PP40-C
$I(t) = (3.11 \pm 0.03).t$ for PP40-H

As it can be seen above these two samples have different slopes.

According to the fitted parameters in table 2, the rate constants T_2 are different so during the first 250 seconds the red component increases with a intensity multiplication factor of 7.5 for PP40-H in comparison to intensity multiplication factor of 4.3 for PP40-C. Figure 4 and table 3 show the evolution of the blue component and the fitting parameters. The decay parameters T_1 and T_2 have higher values for PP40-C than for PP40-H. The consequence is that the emission from the sample PP40-H decreases more rapidly than the CL intensity of the sample PP40-C.

According to the parameter used to compare quartz grains in archaeological ceramics
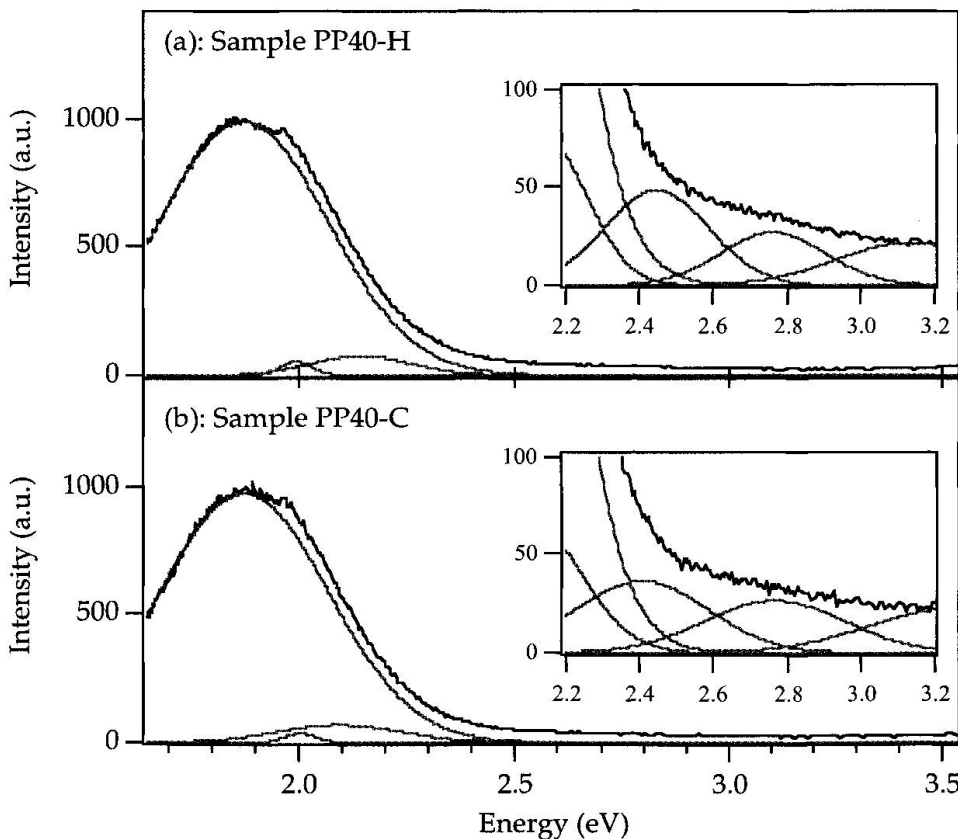

Fig. 2   Polarised cathodoluminescence spectra of a natural quartz with a zoom on the blue range: Luminescence polarised perpendicular (a) and parallel (b) to c-axis. The magnification is x1000 and the analytical surface S is 0.013 mm².
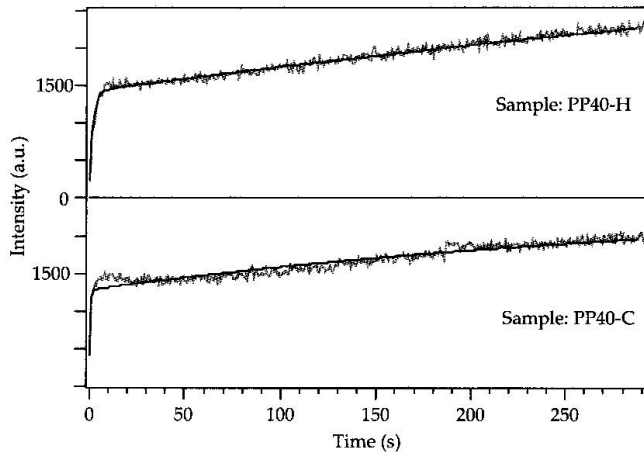
Fig. 3 Evolution of the CL-signal of the red component at 1.88 eV. Experimental curves grey; curve fitting black. The fitting equation was: $I(t) = B_L - I_1.exp(-t/T_1) - I_3.exp(-t/T_2)$ where B_L, I_1, I_2, T_1 and T_2 are the fitting parameters.

(Picouet, 1997; Picouet et al., 1999), the ratio (R) between the area of the blue component (between 2.66–2.86 eV) and the red component (between 1.80–2.00 eV) was established. The spectra were recorded in the linear range. Figures 5a and 5b show the results of the ratio R of PP40-C and PP40-H as a function of the analytical surface S. In this figure it is possible to see that both samples have the same evolution shape. For the small values of S (S = 0.0018 mm²) the ratio R_H is 0.024 ± 0.001 (PP40-H) and the ratio R_C is 0.019 ± 0.001 (PP40-C), the error bars are not overlapping as for the other values of S, there is a divergence between the two ratios. The fitting equation in figure 5a is a single exponential function but it did not provide a very good fit result with a test value
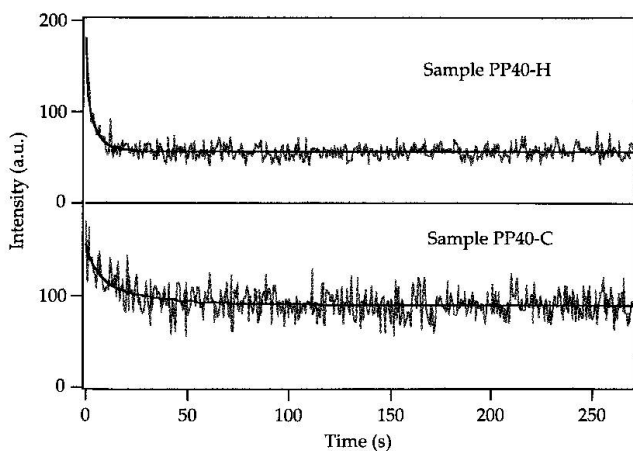

Fig. 4 Evolution of the CL-signal of the blue component at 2.76 eV. Experimental curves grey; curve fitting black. The fitting equation was: $I(t) = B_L + I_1*exp(-t/T_1) + I_2*exp(-t/T_2)$ where B_L, I_1, I_2, T_1 and T_2 are the fitting parameters.

Tab. 2 Parameters of the best-fit of the CL-signal evolution by the following equation: $I(t) = B_L - I_1*exp(-t/T_1) - I_2*exp(-t/T_2)$; where $I(t)$ is the intensity at time t, I_1 and I_2 are intensities constants and T_1 and T_2 are the rate constant. Rate constants are smaller for PP40-H in comparison with PP40-C.

	Red Component at 1.88 eV	
	PP40-C	PP40-H
B_L	2563 ± 192	3532 ± 531
I_1	1234 ± 164	1949 ± 505
T_1	359 ± 96	476 ± 218
I_2	860 ± 5	1165 ± 63
T_2	0.69 ± 0.04	2.03 ± 0.12

Tab. 3 Parameters of the best-fit of the CL-signal evolution by the following equation: $I(t) = B_L + I_1*exp(-t/T_1) + I_2*exp(-t/T_2)$; where $I(t)$ is the intensity at time t, I_1 and I_2 are intensities constants at zero time and T_1 and T_2 are the decay constant. Decay constants are smaller for PP40-H in comparison with PP40-C.

	Rlue Component at 2.76 eV	
	PP40-C	PP40-H
B_L	90 ±3	57 ± 2
I_1	28 ± 10	72 ± 26
T_1	28 ± 4	5 ± 1
I_2	40 ± 3	51 ± 4
T_2	6.1 ± 2.0	0.9 ± 0.3

(Chi-square : CQ) of 0.0019 for PP40-C and PP40-H. A better fit is shown in figure 5b (CQ is 0.0014 for PP40-C and 0.0013 for PP40-H) but the fit equation is more complicated and a physical interpretation is not obvious. However, more R data in the range of S = 0.02–0.2 mm² will help to resolve the fitting problem.

Interpretation

In our results the blue band is much less intense, in comparison to the red component, and the most obvious effects are seen in latter case. The CL-spectra of PP40-H and PP40-C are comparable and the results of the gaussian fitting gave similar values. But the evolution with beam exposure time shows differences between the two samples PP40-H and PP40-C. To explain these differences several effects such as the surface conductivity of the samples, the irradiation-induced electric field or the irradiation induced heat can be considered.

As the two thin sections have been coated with carbon following the same procedure, it is expected that the surface conductivity of both samples have to be very similar. According to STEVENS-KALCEFF and PHILLIPS (1995) the irradiation-in-
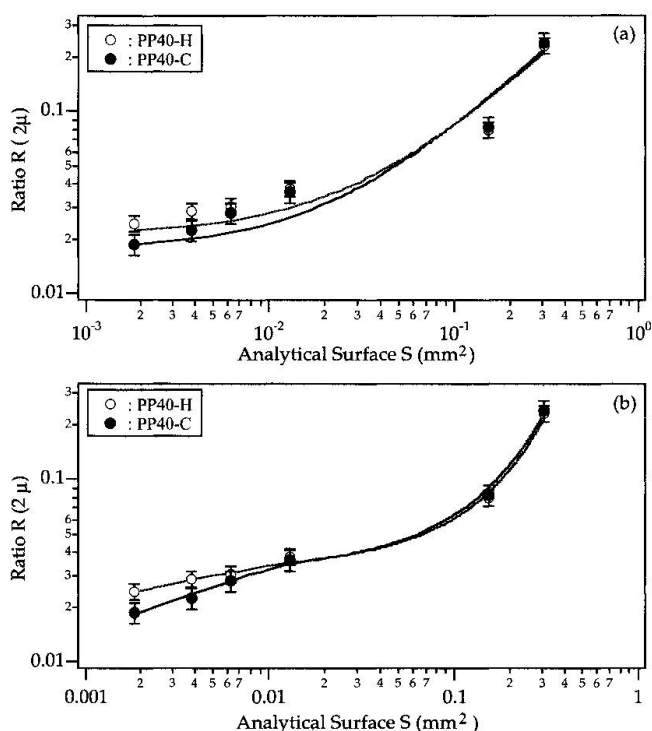
Fig. 5   Ratio R as a function of the analytical surface S. Both axis are in a logarithmic scale and the error bars for R are given in 2σ. The thin curve is for PP40-C, the thick curve is for PP40-H. (a) fit function : $f(x) = K_0 + K_1.exp(-K_2.x)$. (b) fit function : $f(x) = exp[K_0 + K_1.exp(-K_2.x) + K_3.exp(-K_4.x)]$ where the K_i are the fitting parameters.

duced electric field is more significant than irradiation induced heat and the evolution of the red component at 1.91 eV can be correlated to the modifications of trapped charges like hydroxyl (–OH) bonds) or peroxy linkage precursor ($[SiO_5]^-$) which became NBOHC center ($[SiO_4]^+$) by electron-induced irradiation. The evolution of the CL-signal at 2.71 eV is also well described by STEVENS-KALCEFF et al. (1996) which propose that the observed changes result from electromigration of oxygen under the influence of the electrical fields induced by charge trapping at pre-existent or irradiation induced defects.

Figure 3 shows that the crystal perpendicular to the c-axis (PP40-H) is more sensitive to beam damage. In other words if we consider that both samples have the same content of trapped charges, the electron beam induced field is less effective on the PP40-C sample to create NBOHC center. Simultaneously the decrease of the blue emission is much stronger in PP40-H than for PP40-C showing that the electromigration of oxygen is more important in PP40-H.

According to RAMSEYER et al. (1990) the hypothesis that oxygen ions diffuse to the surface along lattice channel parallel to c-axis can explain

the difference observed in CL-signal evolution between samples PP40-H and PP40-C. In addition, the two fittings in Figures 5a and 5b show that there are some differences in the ratio R between the two samples for the small analytical surface ($S < 0.013$ mm^2). In this case the electron-induced irradiation is correlated with the size of the analytical surface. The electron irradiation induced effects increase as the analytical surface is reduced.

Conclusions

Changes in the CL signal observed between the same crystal sample cut perpendicular and parallel to the c-axis are related to the electron irradiation which depend on the experimental conditions. Photoluminescence experiments on the same samples with an ultraviolet laser (excitation at 266 or 355 nm) will be conducted, to avoid the electron beam effects, and to provide complementary information about the crystal defects. For the experimental conditions chosen (PICOUET, 1997; PICOUET et al., 1999) with 20 kV acceleration voltage and 0.15 μA sample current at room temperature and with an analytical surface greater than 0.013 mm^2 variations are small and can be used to compare quartz grains included in archaeological ceramics.

References

BRUHN, F., BRUCKSCHEN, P., MEIJER, J., RICHTER, D.K, STEPHAN, A. and VEIZER, J. (1996): Cathodoluminescence investigations and trace element analysis of quartz by micro-PIXE: implication for diagenic and provenance studies in sandstones. Canad. Mineralogist 34, 1223–1232.

DEMARS, C., PAGEL, M., DELOULE, E. and BLANC, P. (1996): Cathodoluminescence of quartz from sandstones: Interpretation of the UV range by determination of trace element distribution and fluid inclusion P–T–X properties in authigenic quartz. Amer. Mineralogist 81, 891–901.

GORTON, N.T., WALKER, G. and BURLEY, S.D. (1997): Experimental analysis of the composite blue cathodoluminescence emission in quartz. J. Luminescence 72–74, 669–671.

HABERMANN, D., GÖTZE, J., NEUSER, R.D. and RICHTER, D.K. (1999): Case studies of quartz, calcite and apatite. Zbl. Geol. Palaeont. Teil I, 1997, 1275–1284.

IKEYA, M. (1993): New Applications of Electron Spin Resonance: Dating, Dosimetry and Microscopy. Singapore: World Scientific.

LUFF, B.J. and TOWNSEND, P.D. (1990): Cathodoluminescence of synthetic quartz. J. Phys. Condensed Matter 2, 8089–8097.

MATTER, A. and RAMSEYER, K. (1985): Cathodoluminescence microscopy as a tool for provenance studies of sandstones. In: ZUFFA, G.C. (ed.): Provenance of Arenites. Riedel Publ. Co., Boston, 191–211.

MUNEKUNI, T., YAMANAKA, Y., SHINOGAICHI, Y., TOHMON, Y., OHKI, Y., NAGASAWA, K. and HAMA, Y. (1990): Various types of non-bridging oxygen hole center in high-purity silica glass. J. Appl. Phys. 68, 1212–1216.

OWEN, M.R. (1991): Application of cathodoluminescence to sandstone provenance. In: BARKER, C.E. and KOPP, O.C. (eds): Luminescence Microscopy and Spectroscopy: Qualitative and Quantitative Applications. SEPM Short Course 25, 67–75.

PICOUET, P. (1997): Application de la cathodoluminescence à l'étude des céramiques modernes et archéologiques. Ph.D. Thesis No. 1160. University of Fribourg (Switzerland).

PICOUET, P., MAGGETTI, M., PIPONNIER, D. and SCHVOERER, M. (1999): Cathodoluminescence spectroscopy of quartz grains as a tool for ceramic provenance. J. Archaeol. Sci. (in press).

RAMSEYER, K., BAUMANN, J., MATTER, A., and MULLIS, J. (1988): Cathodoluminescence colour of alpha-quartz. Mineral. Mag. 52, 669–677.

RAMSEYER, K. and MULLIS, J. (1990): Factors influencing short-lived blue cathodoluminescence of α-quartz. Amer. Mineralogist 75, 791–800.

REMOND, G., CESBRON, F., CHAPOULIE, R., OHNENSTETTER, D., ROQUES-CARMES, C. and SCHVOERER, M. (1992): Cathodoluminescence applied to microcharacterisation of mineral materials: A present status in experimentation and interpretation. Scanning Microscopy International 6, 23–68.

STEVENS-KALCEFF, M.A. and PHILLIPS, M.R. (1995): Cathodoluminescence microcharacterization of the defect structure of quartz. Phys. Rev. B 52, 3122–3134.

STEVENS-KALCEFF, M.A., PHILLIPS, M.R. and MOON, A.R. (1996): Electron irradiation-induced changes in the surface topography of silicon dioxide. J. Appl. Phys. 80, 1–7.

ZINKERNAGEL, U. (1978): Cathodoluminescence of quartz and its application to sandstone petrology. Contrib. Sedimentology 8, 1–69.